Climate change and emissions impacts on atmospheric PAH transport to the Arctic – Supporting Information

Carey L. Friedman[1], Yanxu Zhang[2] and Noelle E. Selin[3]

[1][Center for Global Change Science, Massachusetts Institute of Technology, Cambridge, Massachusetts]

[2][School of Engineering and Applied Sciences, Harvard University, Cambridge, Massachusetts]

[3][Engineering Systems Division and Department of Earth, Atmospheric, and Planetary Science, Massachusetts Institute of Technology, Cambridge, Massachusetts]

Correspondence to: C. L. Friedman (clf@mit.edu)

Table of Contents **Page**

Table of Contents, continued **Page**

Mean January 2000 PYR concentration (ng/m^3)	*Global*	*NH*	*ML*	*Arctic*
Using monthly average OH, O_3, OC, and BC	0.0694	0.123	0.145	0.0897
Using daily average OH, O_3, OC, and BC	0.0708	0.125	0.148	0.0899
% Difference	+1.9	+2.0	+2.1	+0.21

Table S1. Difference between global, northern hemisphere, northern hemisphere mid-latitude (5-60°N), and Arctic (60-90°N) mean PYR concentrations (ng m^{-3}) for January 2000 when monthly (top) versus daily (bottom) mean oxidant and aerosol concentrations are used as input to the PAH simulation. PYR was used as a test PAH, given its semivolatility and thus sensitivity to changes in both oxidants and particles.

Re-emissions model

Given minimal data on the global distribution of surface concentrations of PAHs and their exchange with the air, the re-emissions model is a simple steady-state level-III fugacity model. Surface concentrations are static, while partition coefficients are re-calculated dynamically on the atmospheric model time step, according to surface and air temperature changes. The re-emissions model has two components: a soil-air exchange model, and a vegetation-air exchange model.

Development of soil-air exchange model (derived primarily from Mackay and Paterson[1]; values of constants are given in Table S2):

Re-emissions from soils are generated as follows: (1) global soil concentration fields are created by multiplying annual simulated deposited mass for each PAH by its "soil deposition storage quotient" (i.e., number of years-worth of atmospheric deposition measured in top 5 cm of soils)[2], and distributing this mass throughout the top 5 cm; (2) air-soil fugacity gradients[1] are calculated using global soil organic carbon fractions generated with a version of the CASA biogeochemical model previously coupled to GEOS-Chem[3]; (3) fluxes and fugacity gradients are constrained to observations[4-6].

Soil storage quotients are 2.6 years for PHE, 10 years for PYR, and 9.4 years for BaP. Resulting soil concentrations were used for all four climate/emissions scenarios. A fraction of this concentration was assumed lost to degradation (at a rate of R_{deg}; Table S2). The fugacities (units of Pa) in the soil (F_{soil}) and the air (F_{air}) were then calculated[1]:

$$F_{soil} = \frac{C_{soil} \times R \times T_{surf}}{K_{SA}}$$

$$F_{air} = C_{air} \times R \times T_{air}$$

where R is the ideal gas constant (m^3 Pa K^{-1} mol^{-1}), T_{surf} is the Earth's surface skin temperature (K), and T_{air} is surface-level air temperature (K), and soil and air concentrations (C_{soil} and C_{air}, respectively) are in units of mol/m^3. K_{SA} (mol m^{-3} soil / mol m^{-3} air) is a soil-air partition coefficient calculated following previously described methods[7-9]:

$$K_{SA} = 1.5 \times f_{OC} \times K_{OA}$$

where f_{OC} is the fraction of organic carbon in the soil and K_{OA} is the temperature-dependent octanol-air partition coefficient. The f_{OC} is calculated by (1) combining annual mean carbon mass from all carbon pools simulated by the Global Terrestrial Mercury Model (GTMM), which is a version of the CASA biogeochemical model[10] coupled to the GEOS-Chem atmospheric mercury model[3]; (2) assuming this carbon mass extends to 30 cm[10] to create a soil carbon concentration; (3) assuming a mean soil bulk density[11] of 1300 kg/m^3 to calculate a soil organic carbon fraction (g C/g soil).

The soil-air flux ($Flux_{SA}$) is then calculated as follows:

$$Flux_{SA} = DS \times (F_{soil} - F_{air}) \times 24 \times MW_{PAH} \times 10^{12}$$

where $Flux_{SA}$ is in units of ng/m^2/day, DS is diffusivity through the soil (mol m^{-2} h^{-1} Pa^{-1}), and MW_{PAH} is the PAH molecular weight (kg/mol).

DS is calculated by:

$$DS = \frac{1}{\left(1/DSA + PL/(DAD + DWD)\right)}$$

where DSA is the air-side boundary layer diffusion parameter (mol/h/Pa;), PL is the soil diffusion path length (m), DAD is the diffusion parameter between soil particles and soil air (mol/h/Pa), and DWD is the diffusion parameter between soil pore water and particles (mol/h/Pa). Diffusion parameters are calculated as follows:

$$DSA = K_{SA} Z_{air}$$

$$DAD = BA \times Z_{air}$$

$$DWD = BW \times Z_{water}$$

where BA is the molecular diffusivity in air (m^2/h), BW is the molecular diffusivity in water (m^2/h), and Z_{air}, Z_{soil}, and Z_{water} are the fugacity capacities (mol/m^3/Pa) in air, soil, and water:

$$Z_{air} = \frac{1}{RT_{air}}$$

$$Z_{water} = \frac{1}{K_{AW} R T_{surf}}$$

Net fluxes (the sum of monthly mean positive and negative fluxes), when positive, are added to primary emissions to calculate total emissions.

Development of vegetation-air exchange model (derived primarily from Cousins and Mackay[1, 12, 13]; values of constants are given in Table S2):

Re-emissions from vegetation are generated by considering fugacity gradients between leaf surfaces and air. Vegetation PAH concentrations (C_{leaf}) were generated by distributing the annual simulated deposited mass for each PAH throughout a general leaf surface thickness (d_{leaf}) of 2e-6 m and an arbitrary leaf surface area such that concentrations were of the same order of magnitude as those previously reported[14, 15] (i.e., PHE concentrations in the hundreds, PYR in the tens, and BaP between 1 and 10). The resulting concentrations were used for all four climate/emissions scenarios. A temperature-dependent octanol-water partition coefficient (K_{OW}, unitless) was then estimated from K_{OA} and K_{AW}:

$$K_{OW} = K_{OA} K_{AW}$$

and a leaf surface – air partition coefficient (K_{LA}) was also calculated from the K_{OA} by assuming an octanol-equivalent volume fraction[12] (f_{oct}) in the leaf surface of 0.8:

$$K_{LA} = f_{oct} K_{OA}$$

Fugacities (Pa) in the leaf surface (F_{leaf}) and air (as above) were then calculated from their respective concentrations (mol/m^3):

$$F_{leaf} = \frac{C_{leaf} \times R \times T_{surf}}{K_{LA}}$$

The vegetation-air flux (ng/m^2/d) was derived from the fugacity gradient:

$$Flux_{VA} = DLA \times (F_{leaf} - F_{air}) \times 24 \times MW_{PAH} \times 10^{12}$$

where DLA (mol/Pa/h) is the diffusion parameter for gas phase leaf surface – air transfer. DLA is calculated by:

$$DLA = \frac{1}{1/DC + 1/DAB_f}$$

where DC (mol/Pa/h) is cuticle diffusions and DAB_f (mol/Pa/h) is the boundary layer diffusion. DC is given by:

$$DC = As \times L \times Uc \times Z_{leaf}$$

where As is the area of the land surface (m^2), L is the leaf area index (m^2/m^2), Uc is the cuticle mass transfer coefficient (m/h), and Z_{leaf} is the fugacity capacity of the leaf ($mol/m^3/Pa$). Uc is determined by:

$$Uc = 3600 \times Pc \times 1/K_{AW}$$

where Pc is the cuticle permeance (m/s) given by:

$$\log(Pc) = \frac{((0.704 \times \log(K_{OW}) - 11.2) + (-3.47 - 2.79 \times \log(MW_{PAH}) + 0.970 \times \log(K_{OW}))}{2}$$

Z_{leaf} is calculated as follows:

$$Z_{leaf} = \frac{K_{LA}}{RT_{surf}}$$

DAB_f is given by:

$$DAB_f = UAB_f \times Z_{air}$$

where UAB_f is a mass transfer coefficient for surface-air boundary layer diffusion (m/h) and Z_{air} is as above ($mol/m^3/Pa$).

Vegetation emissions (kg/s) are then calculated by:

$$Em_{veg} = \frac{Flux_{VA} \times A \times LAI}{24 \times 3600 \times 10^{12}}$$

where A is the area of the grid box (m^2) and LAI is the leaf area index (cm^2 leaf surface/cm^2 GEOS-Chem gridbox) given by the NOAA Advanced Very High Resolution Radiometer (AVHRR) satellite. Emissions are added to primary emissions when $Flux_{VA}$ is positive.

Vegetation flux observations are, to our knowledge, unavailable in the literature.

Compound	Metric	Lat.	Long.	Observation period	Observation Values	Simulated Value	Observation reference
PHE	Fugacity ratio (unitless)	41.4-42.4 N	2.7 W-2.1 E	6/2006	10 to 600*	37	(a)
				11/2006		3	(a)
				9/2007		19	(a)
	Flux (ng/m^2/day)	38.5 – 41.1 N	115.4 – 118.1 E	Fall 2007	-13 (median); -99 to 268 (range)	-3	(b)
				Winter 2007	-115 (median); -348 to -10 (range)	-62	(b)
				Spring 2008	-11 (median); -86 to 250 (range)	27	(b)
				Summer 2008	92 (median); 6 to 796 (range)	218	(b)
	Fugacity fraction (unitless)	22 – 23.8 N	112.4 – 114.2 E	9/2001	0.02 – 0.11	0.98	(c)
PYR	Fugacity ratio (unitless)	41.4-42.4 N	2.7 W-2.1 E	6/2006	10-150*	46	(a)
				11/2006		2	(a)
				9/2007		23	(a)
	Flux (ng/m^2/day)	38.5 – 41.1 N	115.4 – 118.1 E	Fall 2007	-3 (median); -10 to 6 (range)	-2	(b)
				Winter 2007	-11 (median); -37 to -0.8 (range)	-5	(b)
				Spring 2008	-7 (median); -25 to 5 (range)	1	(b)
				Summer 2008	2 (median); -12 to 31 (range)	45	(b)
	Fugacity fraction	22 – 23.8 N	112.4 – 114.2 E	9/2001	0-0.08	0.97	(c)
BaP	Fugacity ratio (unitless)	41.4-42.4 N	2.7 W-2.1 E	6/2006	0.9-3*	0.11	(a)
				11/2006		0.07	(a)
				9/2007		0.03	(a)
	Flux (ng/m^2/day)	38.5 – 41.1 N	115.4 – 118.1 E	Fall 2007	-0.01 (median); -0.04 to NA (range)	-0.03	(b)
				Winter 2007	-0.02 (median); -0.07 to NA (range)	-0.001	(b)
				Spring 2008	-0.01 (median); -0.06 to NA (range)	-0.02	(b)
				Summer 2008	-0.01 (median); -0.04 to NA (range)	-0.07	(b)

Table S2. Comparison of simulated re-emissions fluxes, fugacity ratios, and fugacity fractions to observed. Positive fluxes are in the direction of soil-to-air, negative fluxes are air-to-soil. Fugacity ratios are defined as the fugacity in the soil divided by the fugacity in the air. Fugacity fractions are defined as the fugacity in the soil divided by the sum of the fugacities in soil and air. Observations are from (a) Cabrerizo et al., 2011[5]; (b) Wang et al., 2011[4]; and (c) Liu et al., 2011[6]. The evaluation of the flux model was completed

using NASA GEOS5 meteorology and for all observation data except those from Liu et al., simulated values were derived from the meteorological months corresponding to the reported sampling periods. For comparisons to Liu et al. data, mean simulated values from September 2005-2009 were used. *Values are approximations derived from plots in cited work. Our simulations capture the reported seasonal variation (largest fugacity ratios in June, followed by September, and then November). N.A. = not available.

Parameter	Description	PHE	PYR	BaP	Ref
log K_{OA}	Octanol-air partition coefficient	7.64	8.86	11.48	a
log K_{BC}	Black carbon-air partition coefficient	10.0	11.0	13.9	b
log K_{AW}	Air-water partition coefficient	-2.76	-3.27	-4.51	a
$\Delta_{OA}H$ (kJ/mol)	Enthalpy of phase transfer from gas phase to OC	-74	-87	-110	c
$\Delta_{BC}H$ (kJ/mol)	Enthalpy of phase transfer from gas phase to BC	-74	-87	-110	c
$\Delta_{AW}H$ (kJ/mol)	Enthalpy of phase transfer from water to air	47	43	43	c
k_{OH} (cm^3/molec/s)	Reaction rate constant for oxidation of gas phase with OH	2.70e-11	5.00e-11	5.00e-11	d, e
A (s^{-1})	Kinetic parameter for ozonation of PAHs on octanol and decanol	5e-4	7e-4	5.5e-3	f
B (molec/cm^3)	Kinetic parameter for ozonation of PAHs on octanol and decanol	2.15e15	3e15	2.8d15	f
k_{SA} (m/h)	Air-side mass transfer coefficient over soil	1.0	1.0	1.0	g
BA (m^2/h)	Molecular diffusivity in air	0.04	0.04	0.04	g
BW (m^2/h)	Molecular diffusivity in water	4e-6	4e-6	4e-6	g
R_{deg} (h^{-1})	Degradation rate in soil	3.5e-5	3.5e-5	3.5e-5	g
PL (m)	Soil path length (half of soil depth)	0.025	0.025	0.025	g
UAB_f (m/h)	Leaf surface transfer velocity	9	9	9	h
ρ_{oct} (kg/m^3)	Density of octanol	820			b
ρ_{BC} (kg/m^3)	Density of BC	1000			b
τ_{OCBC} (d)	Lifetime of hydrophobic OC and BC before converting to hydrophilic	1.15			i
f_{oct}	Volume fraction of octanol equivalent in leaf surface	0.8			g
d_{leaf} (m)	Leaf surface thickness	2e-6			h

Table S3. Physicochemical constants used in model for PHE, PYR, and BaP. References: (a) Ma et al., 2010[16]; (b) Lohmann and Lammel, 2004[17]; (c) Schwarzenbach et al., 2003[18]; (d) Brubaker and Hites, 1998[19]; (e) U.S. EPA Episuite software[20]; (f) Kahan et al., 2006[21] (g) Mackay and Paterson, 1991[1]; (h) Cousins and Mackay, 2001[12]; (i) Park et al., 2003[22].

Particles and oxidants under FE OC and BC emissions result from four source types: biofuel, biomass burning (including wildfires), fossil fuel, and biogenic (OC only)[22]. For FE and FCFE simulations, we use 2050 anthropogenic OC and BC emissions (i.e., from biofuel, biomass burning, and fossil fuel sources) estimated under the IPCC's A1B scenario based on previously reported methods[23-26]. The control emissions, minimum and maximum scaling factors for future global emissions, and the mean percent changes in global OC and BC emissions are shown in Table S3. Declining emissions generally result in decreases in OC and BC concentrations.

Surface O_3 and OH concentrations increase, mostly from changes in anthropogenic NO_X and methane. Model simulations for the purpose of investigating O_3 and OH concentrations under future emissions and climate scenarios have been described extensively previously[24, 27]. Here we reproduce a summary of global O_3 precursor emissions under the control simulation, their scaling factors for 2050, and the mean percent change in total emissions in 2050 (Table S4)[24]. In addition to the species in Table S4, global mean methane concentrations are specified at 1750 ppb with a 5% interhemispheric gradient, based on observations. As methane is projected to rise to 2400 ppb by 2050 in the A1B scenario, a globally uniform methane concentration of 2400 ppb is used in the model for all future anthropogenic emissions scenarios.

Global surface concentrations in the control and future emissions scenarios are summarized in Figs. S5-S8 and Table S5.

Emissions source	*Control (Mg)*	*Scaling factors (Min-Max)*	*% Δ Global, 2050-2000*
		BC	
Biofuel	1.6×10^6	0.179 - 1.726	-60
Biomass burning	1.7×10^6	0.360 - 1.851	-14
Fossil fuel	3.0×10^6	0.212 - 2.977	-32
		OC	
Biofuel	6.3×10^6	0.160 - 1.615	-58
Biomass burning	1.6×10^7	0.354 - 1.702	-18
Fossil fuel	3.0×10^6	0.217 - 1.174	-64

Table S4. Global annual emissions of particles under the control (2000) simulation, range of growth factors for 2050 FE and FCFE scenarios (depending on region), and resulting change in global emissions for 2050.

Emissions source	*Control (Mg)*	*Scaling factors (Min-Max)*	*% Δ Global, 2050-2000*
		NO_x (emissions of N)	
Biofuel	2.2×10^6	0.150 - 1.844	-5
Biomass burning	6.5×10^6	0.038 - 6.000	+25
Fertilizer	0.5×10^6	0.748 - 24.833	+80
Fossil fuel	24.6×10^6	0.597 - 18.354	+90
		CO	
Biofuel	176×10^6	0.160 - 1.846	-4%
Biomass burning	459×10^6	0.025 - 13.381	+63%
Fossil fuel	381×10^6	0.416 - 11.862	-5%
		Non-methane volatile organic compounds (NVMOCs; emissions of C)	
Anthropogenic	43×10^6	0.454 - 9.033	+130
Biomass burning	10×10^6	0.025 - 15.250	+66

Table S5. Global annual emissions of O_3 precursors under the control (2000) simulation, range of growth factors for 2050 FE and FCFE scenarios (depending on region), and resulting change in global emissions for 2050.

Particles and oxidants under FC Concentrations of OC, BC, O_3, and OH vary with FC due to changes in biogenic emissions (OC), chemical precursors (O_3 and OH), and meteorology (all). OC emissions increase by 2%. Briefly, the FC simulation considers changes to natural emissions of O_3 precursors, including nonmethane volatile organic compounds (NMVOCs) from vegetation, and NO_x from lightning and soil. These emissions are calculated within the model based on meteorology and hence change with climate scenario. Biogenic emissions of NMVOCs are influenced by temperature and solar radiation. Isoprene emissions increase by 25%, while all other NMVOC emissions increase by 20%. Lightning NO_x, a function of deep convective cloud top, increases by 18% globally, while soil NO_x emissions, a function of vegetation type, temperature, precipitation, fertilizer use, and leaf area index, increase by 8%. The model does not account for stratosphere-troposphere exchange of O_3. The effect of climate on global OH and O_3 has been discussed in detail by Wu et al.[24]

Together, emissions and meteorological changes result in lower surface-level OC and BC and small decreases in OH and O_3 under FC. These changes are summarized in Figs. S5-S8, Table S5).

Simulation			
Control Concentration	*FE (%Δ)*	*FC (%Δ)*	*FCFE (%Δ)*
OC (μg/m^3)			
0.056	-22	-18	-42
BC (μg/m^3)			
0.022	-30	-7	-38
OH (molec/cm^3)			
1e6	+4	-1	+5
O_3 (ppbv)			
34	+16	-2	+14

Table S6. Global surface concentrations of particles (OC and BC) and oxidants (OH and O_3) in the control, and percent change under each future scenario.

	% of total present-day emissions												Future anthropogenic emissions scaling factors (% Δ)				Total 2050 emissions and %Δ from control					
	PHE				PYR				BaP				Same for all PAHs				PHE		PYR		BaP	
Source region	Biomass burning	Vehicle use	Domestic coal	Coke production	Biomass burning	Vehicle use	Domestic coal	Coke production	Biomass burning	Vehicle use	Domestic coal	Coke production	Biomass burning	Vehicle use	Domestic coal	Coke production	Pres. (Mg)	% Δ	Pres. (Mg)	% Δ	Pres. (Mg)	% Δ
E. Asia	60	1	12	19	68	1	7	18	59	1	12	24	-60	-76	-60	-28	16,224	-10	6,501	-9	1,501	-11
S. Asia	85	1	1	<1	83	1	1	<1	89	1	2	1	-6	+13	-6	-28	18,096	-52	6,811	-51	1,204	-55
Europe	39	7	9	3	43	8	6	4	40	4	12	7	0	-98	0	+46	3,814	-6	1,191	-6	268	-1
N. America	22	12	2	1	27	13	1	1	27	10	3	3	0	-99	0	+75	3,020	-11	925	-12	161	-8
Russia	6	4	13	4	5	4	9	5	5	3	18	10	0	-98	0	+75	1,155	-1	382	-1	80	+5

Table S7. Contribution of different anthropogenic source activities to present-day total PAH emissions, factors for scaling anthropogenic emissions to 2050 for each source activity, and present-day total emissions and 2050 changes. Blue cells mark a decrease in emissions; red marks an increase.

	% of total present-day emissions due to wildfire			Future scaling factor (%)	Change in total emissions (% Δ)		
Source region	PHE	PYR	BaP	(all PAHs)	PHE	PYR	BaP
East Asia	1	1	<1	+25	0	0	0
South Asia	9	11	6	+50	+5	+6	+3
Europe	1	1	<1	+200	+2	+1	+1
North America	13	18	10	+88	+12	+16	+9
Russia	24	30	14	+15	+4	+4	+2

Table S8. Contribution of wildfire to present-day emissions, future climate wildfire emissions scaling factors, and 2050 changes due to wildfire.

Sensitivities to assumptions regarding wildfire emissions changes under FC

Given lack of projections for future wildfire activity in East Asia and Russia, we assume wildfire emissions in East Asia increase by half the increase in South Asia, and emissions in Russia increase by half the greatest predicted increase in annual dangerous fire days. These assumptions result in no change in East Asian wildfire emissions from 2000 to 2050, and a small increase in wildfire emissions in Russia from 2000 to 2050 (+2% to +4%; Table S7). If we adjust the scaling factors of these regions by +/-50%, given recent studies finding uncertainties in wildfire emissions within this range[28], we still find no impact on East Asian emissions, reflecting the low contribution of wildfire to total emissions in this region. Adjusting the scaling factor in Russia, however, can increase or decrease the 2000-2050 changes shown in Table S7 by up to 17% (for PYR). In other words, with a +/-50% certainty in the wildfire emissions scaling factors, 2000-2050 Russian emissions could either decrease by as much as 13%, or increase by as much as 21%. Russian emissions, however, account for only a small portion of the global inventory. For example, if we consider only the regions that we scale, Russian emissions account for just 2-3% of the total. Thus, +/-50% changes in Russian emissions projections have virtually no impact on the total 2000-2050 change in emissions under FC (<1%).

	Simulation			
Emissions	***Control (Mg)***	***FE (%Δ)***	***FC (%Δ)***	***FCFE (%Δ)***
		PHE		
Primary (kg)	61,000	-17	+2	-15
Re-emissions: Soil (kg)	12,000	+1	+23	+24
Re-emissions: Vegetation (kg)	180	+80	+28	+139
Total (kg)	72,000	-14	+5	-8
Re-emissions/Total	16%	+3	+3	+6
		PYR		
Primary (kg)	21,000	-18	+2	-16
Re-emissions: Soil (kg)	1800	+1	+28	+29
Re-emissions: Vegetation (kg)	2.3	+154	+33	+274
Total (kg)	23,000	-17	+4	-12
Re-emissions/Total	8%	+2	+2	+4
		BaP		
Primary (kg)	4200	-20	+1	-19
Re-emissions: Soil (kg)	0.32	+13	+48	+67
Re-emissions: Vegetation (kg)	7.4e-10	-63	+214	-52
Total (kg)	4200	-20	+1	-19
Re-emissions/Total	1%	+<1	+<1	+1

Table S9. Global primary, re-, and total annual emissions (kg) in the control and percent change in future simulations. Also shown is percent re-emissions of total, and change in percentage for future simulations.

	PHE			PYR			BaP			
Parameter	Used in model	Lower bound	Upper bound	Used in model	Lower bound	Upper bound	Used in model	Lower bound	Upper bound	Associated References
log K_{OA}	7.64	7.6	7.68	8.86	8.7	8.86	11.48	11.1	11.56	1, 2, 3
log K_{BC}*	10.0	9.24	10.1	11.0	10.45	11.04	13.9	12.9	14.1	4
log K_{AW}	-2.76	-3.0	-2.64	-3.27	-3.34	-3.15	-4.51	-4.85	-4.51	1, 5
Δ_{OA}H (kJ/mol)	-74	-80.62	-52.97	-87	-87.79	-75.89	-110	-110	-85	5, 6
Δ_{BC}H (kJ/mol)	-74	-80.62	-52.97	-87	-87.79	-75.89	-110	-110	-85	5, 6
Δ_{AW}H (kJ/mol)	47	30	60	43	30.5	56	43	43	43	5, 6
k_{OH} (cm^3/molec/s)	2.70e-11	1.3e-11	3.1e-11	5.00e-11	2.03e-11	2.92e-10	5.00e-11	5.00e-11	2.65e-10	7, 8, 9, 10

Table S10. Physicochemical parameters dominating PAH behavior within the atmospheric model: those used within the model and their lower and upper literature-derived values. *Upper and lower limits are calculated using a ratio of reported minimum and maximum $K_{BC\text{-}water}$ partition coefficients and minimum and maximum K_{AW}s. Associated references for this row include sources for both these partition coefficients.

References: (1) Ma et al., 2010[16]; (2) Beyer et al., 2002[29]; (3) Odabasi et al., 2006[30]; (4) Lohmann and Lammel, 2004[17]; (5) Shiu and Ma, 2000[31]; (6) Schwarzenbach et al., 2003[18]; (7) Brubaker and Hites, 1998[19]; (8) U.S. EPA Episuite software[20]; (9) NIST (http://webbook.nist.gov/cgi/cbook.cgi?ID=C50328&Mask=20#Ion-Energetics); (10) Bierman[32]

	Simulation			
	Control (ng m^{-3})	**FE (%Δ)**	**FC (%Δ)**	**FCFE (%Δ)**
PHE				
Global	0.18	-21	+5	-17
NH	0.30	-23	+4	-19
ML	0.36	-24	+4	-19
Arctic	0.15	-6	-2	-8
PYR				
Global	0.041	-25	+2	-23
NH	0.069	-28	+1	-26
ML	0.082	-29	+1	-26
Arctic	0.025	-6	-2	-7
BaP				
Global	0.022	-35	-3	-37
NH	0.039	-37	-3	-38
ML	0.048	-37	-3	-38
Arctic	6.7e-3	-7	-1	-8

Table S11. Global, northern hemisphere, northern hemisphere mid-latitude (5-60°N), and Arctic (60-90°N) mean concentrations (ng m^{-3}) in the present-day control and percent change for each future simulation.

	Simulation			
	Control Deposition/Emissions (kg/kg)	***FE (%Δ)***	***FC (%Δ)***	***FCFE (%Δ)***
PHE				
Gas dry	9%	-11	+2	-10
Particle dry	<1%	-28	-15	-37
Gas wet	<1%	-12	-2	-16
Particle wet	<1%	-56	-10	-62
TOTAL	9%	-11	+1	-11
PYR				
Gas dry	20%	-7	+4	-3
Particle dry	1%	-38	-15	-45
Gas wet	<1%	-9	-1	-11
Particle wet	<1%	-58	-10	-63
TOTAL	22%	-9	+3	-6
BaP				
Gas dry	7%	+25	+20	+47
Particle dry	12%	-20	-4	-24
Gas wet	1%	+15	+12	+25
Particle wet	10%	-28	-2	-31
TOTAL	30%	-10	+3	-7

Table S12. Global deposition (kg) normalized to total (primary + re-) emissions (kg) for each PAH in the control simulation, and the percent change in this ratio for future scenarios.

	Simulation			
	Control Oxidation/Emissions (kg/kg)	***FE (%Δ)***	***FC (%Δ)***	***FCFE (%Δ)***
PHE				
OH oxidation (gas)	90%	+2	-<1%	+2
O_3 oxidation (particles)	<1%	-<1%	-<1%	-<1%
TOTAL	90%	+2	-<1%	+2
PYR				
OH oxidation (gas)	78%	+2	-1	+1
O_3 oxidation (particles)	<1%	-<1%	-<1%	-<1%
TOTAL	78%	+2	-<1%	+2
BaP				
OH oxidation (gas)	41%	+7	+2	+9
O_3 oxidation (particles)	28%	-4	-3	-7
TOTAL	69%	+4	-1	+3

Table S13. Global oxidation (kg) normalized to total (primary + re-) emissions (kg) for each PAH in the control simulation, and the percent change in this ratio for future scenarios.

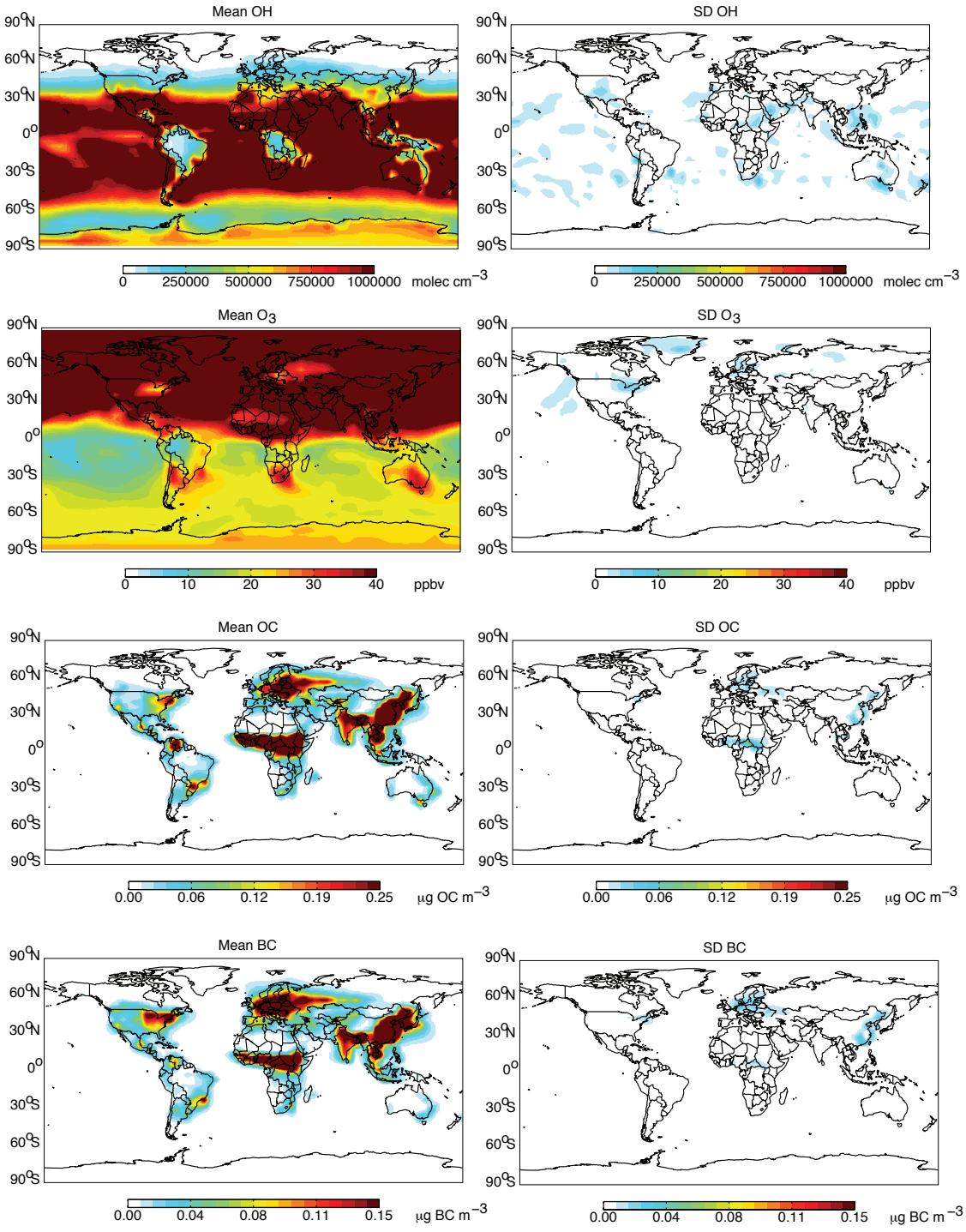

Figure S1. Monthly (January 2000) mean oxidant and aerosol concentrations when averaged over daily values (left panel) and associated standard deviations (right panel). Standard deviations suggest only minor variation in concentrations within a given month for each species. See Table S1 for the effects of averaging on mean PAH concentrations.

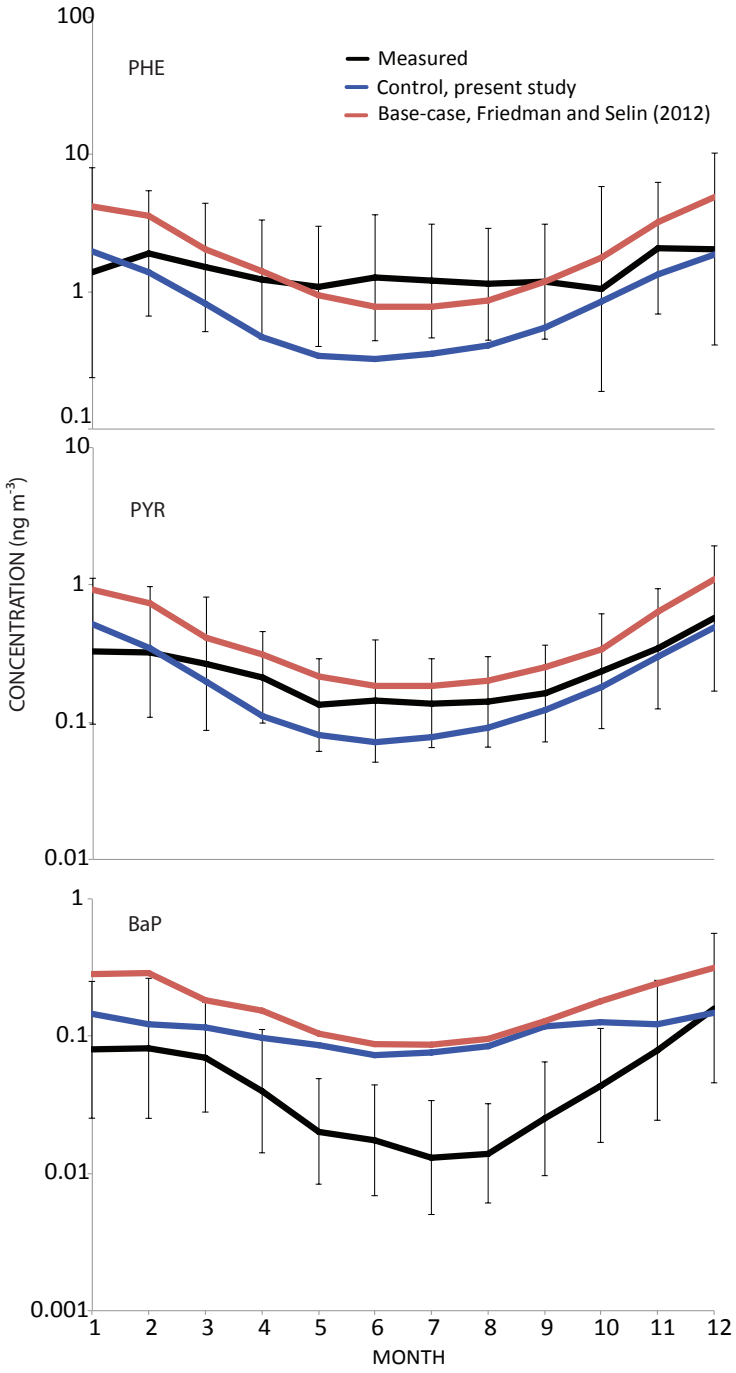

Figure S2. Comparison of non-urban mid-latitude concentrations from the control simulation in the present study to observations and simulated concentrations from Friedman and Selin[33]. Concentrations are monthly geometric means (+/- 1SD) from the non-urban mid-latitude sites (n=15 for PHE, PYR; n=16 for BaP) presented in Table 1 of Friedman and Selin.

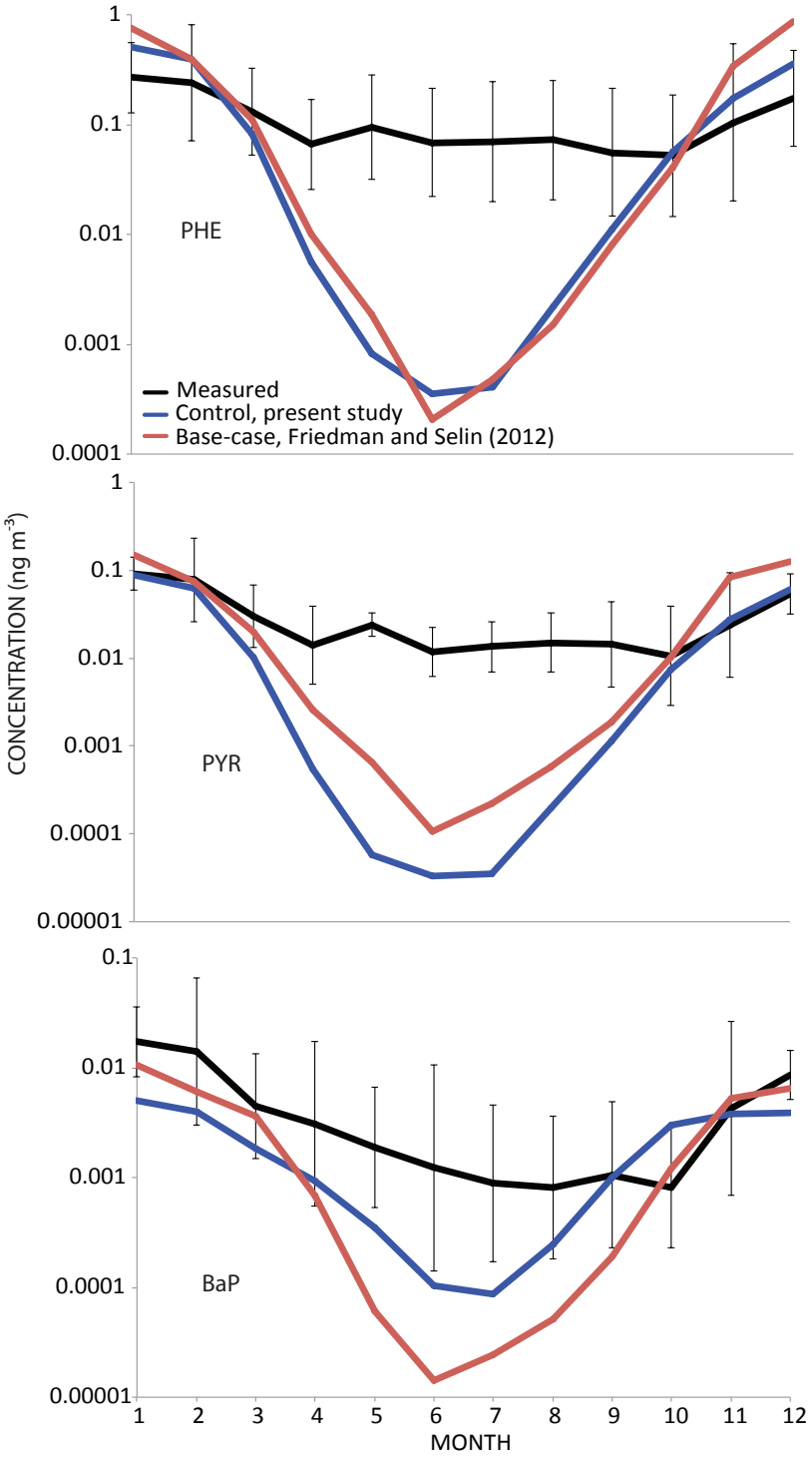

Figure S3. Comparison of Arctic concentrations from the control simulation in the present study to observations and simulated concentrations from Friedman and Selin[33]. Concentrations are monthly geometric means (+/- 1SD) from Arctic sites (n=3) presented in Table 1 of Friedman and Selin[33].

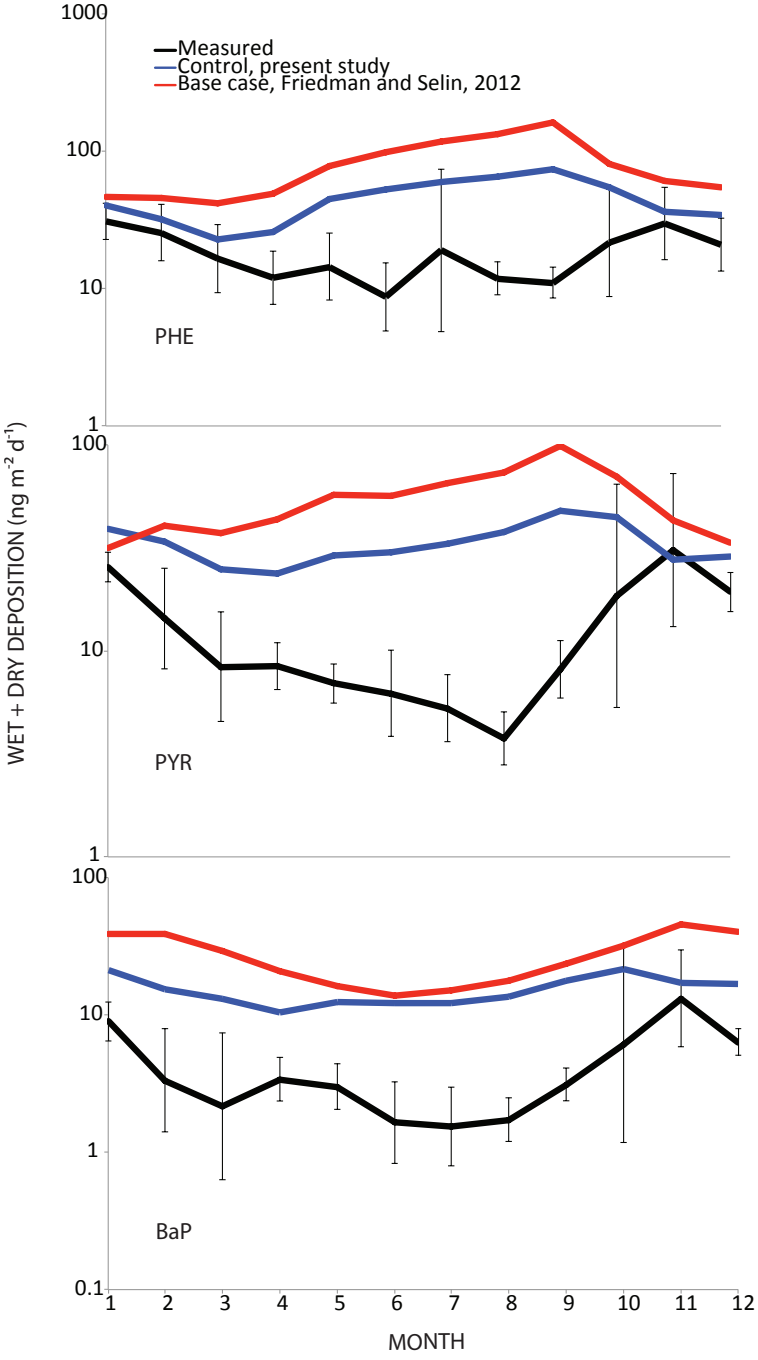

Figure S4. Comparison of deposition from the control simulation in the present study to observations and simulated deposition from Friedman and Selin[33]. Deposition values are monthly geometric means (+/- 1SD) from EMEP sites routinely reporting deposition (n=3) presented in Table 1 of Friedman and Selin[33].

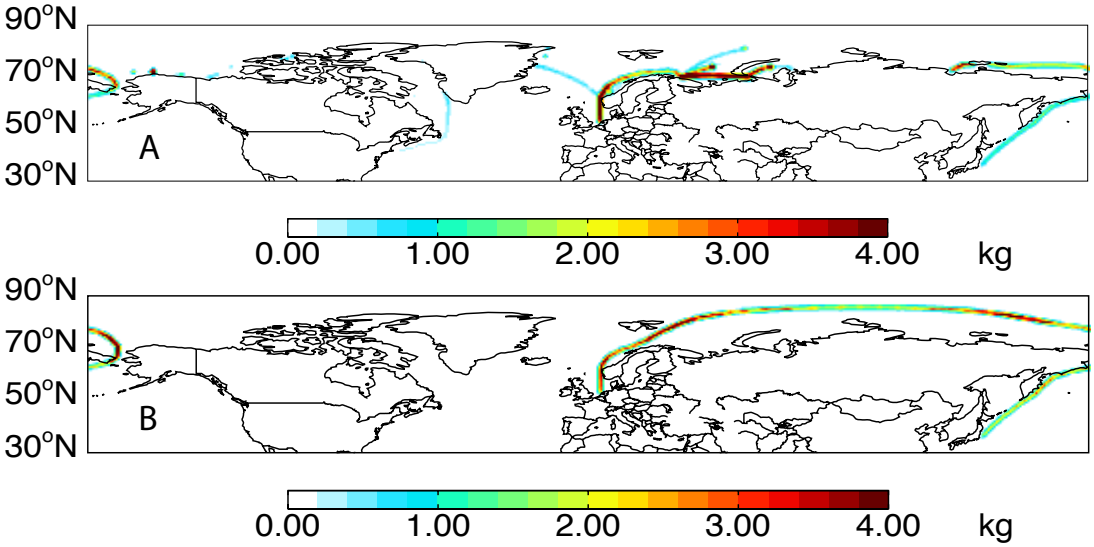

Figure S5. (A) Annual average of monthly emissions from 2050 projected shipping related to oil and gas; (B) average of monthly emissions from July - November 2050 projected transit shipping. Transit shipping is not projected to take place in the Arctic outside of these months.[34]

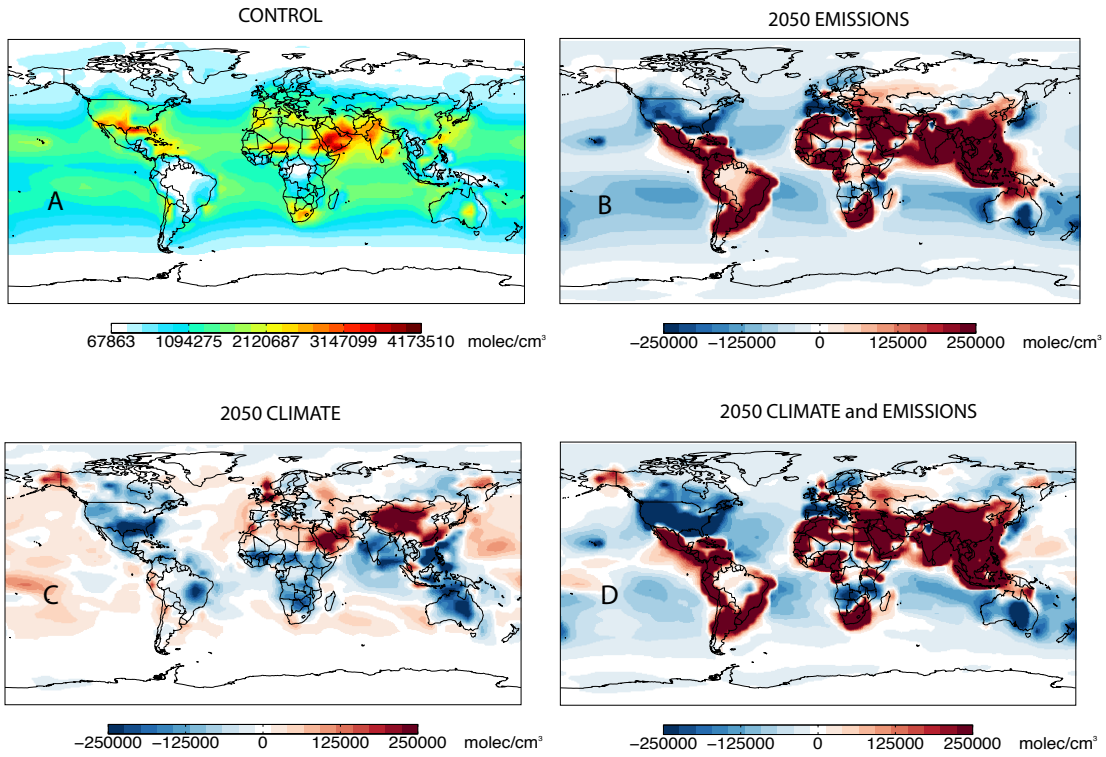

Figure S6. Global concentrations of OH under (A) the control simulation and difference in concentration between the control and simulations under (B) future emissions; (C) future climate, and; (D) future climate and future emissions. Red marks an increase in concentrations, blue marks a decrease.

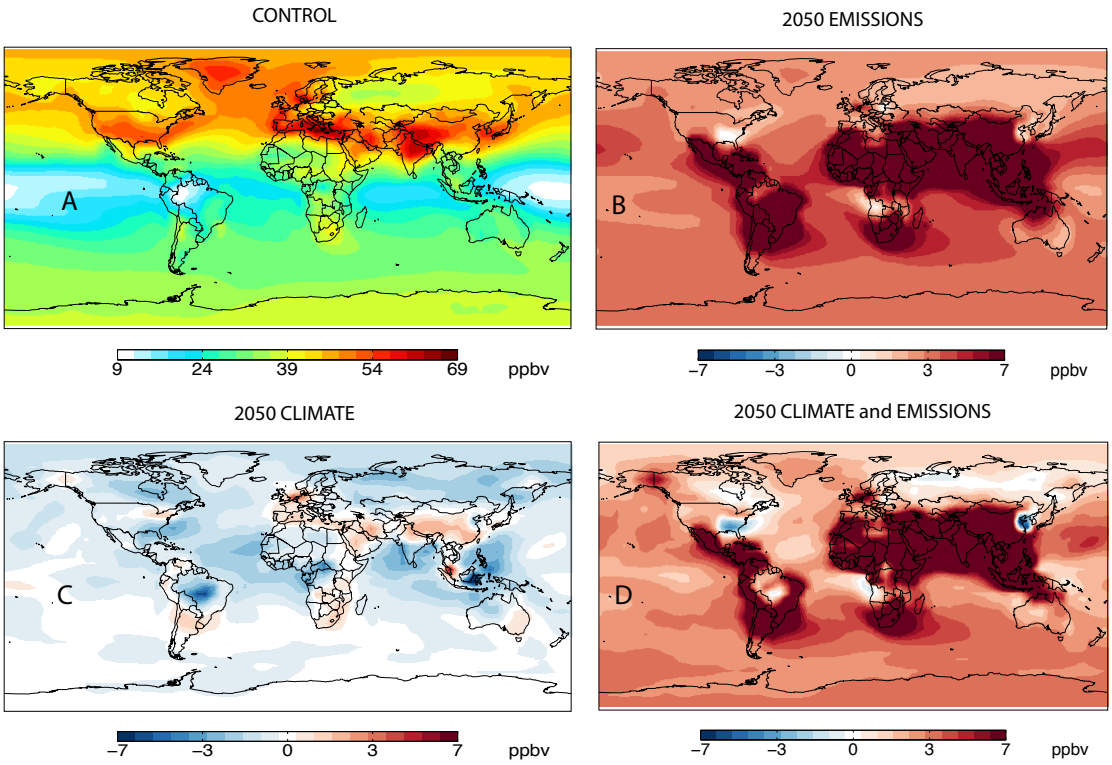

Figure S7. Global concentrations of O_3 under (A) the control simulation and difference in concentration between the control and simulations under (B) future emissions; (C) future climate, and; (D) future climate and future emissions. Red marks an increase in concentrations, blue marks a decrease.

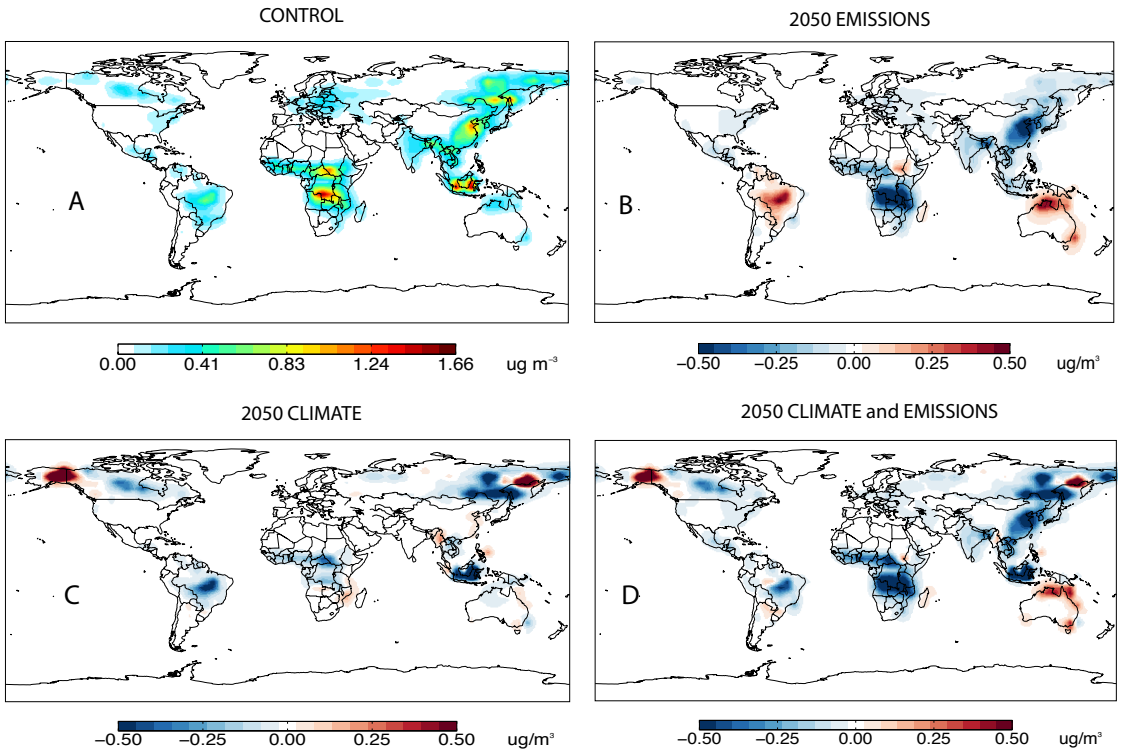

Figure S8. Global concentrations of OC under (A) the control simulation and difference in concentration between the control and simulations under (B) future emissions; (C) future climate, and; (D) future climate and future emissions. Red marks an increase in concentrations, blue marks a decrease.

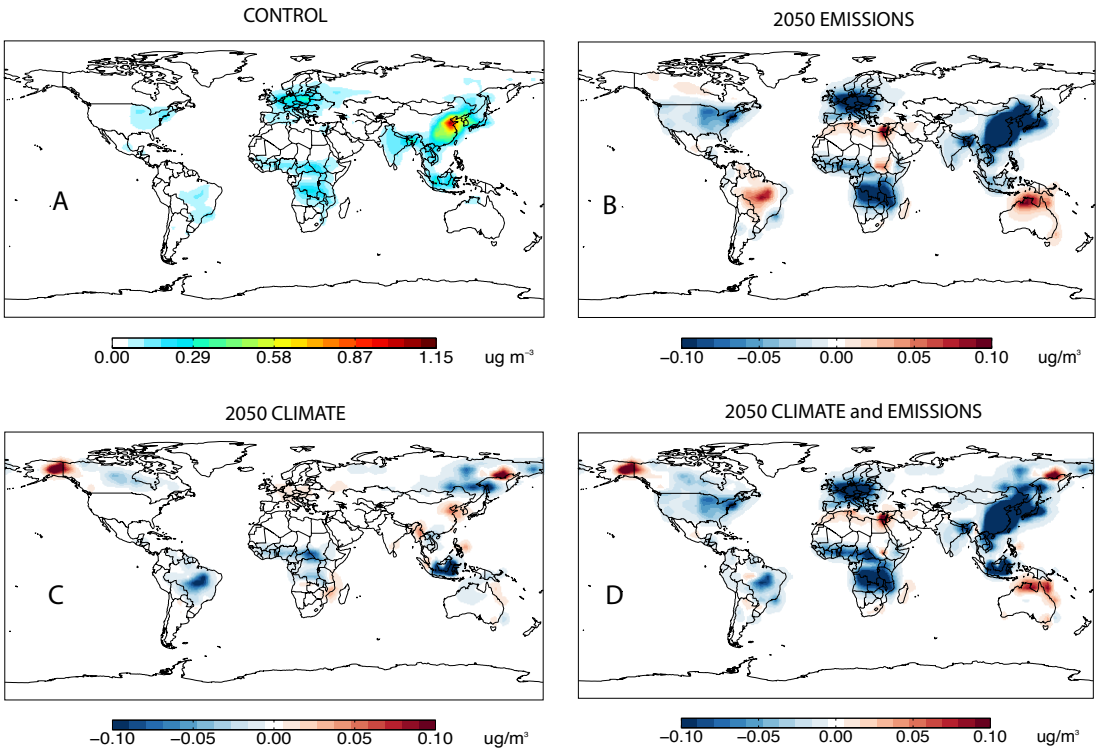

Figure S9. Global concentrations of BC under (A) the control simulation and difference in concentration between the control and simulations under (B) future emissions; (C) future climate, and; (D) future climate and future emissions. Red marks an increase in concentrations, blue marks a decrease.

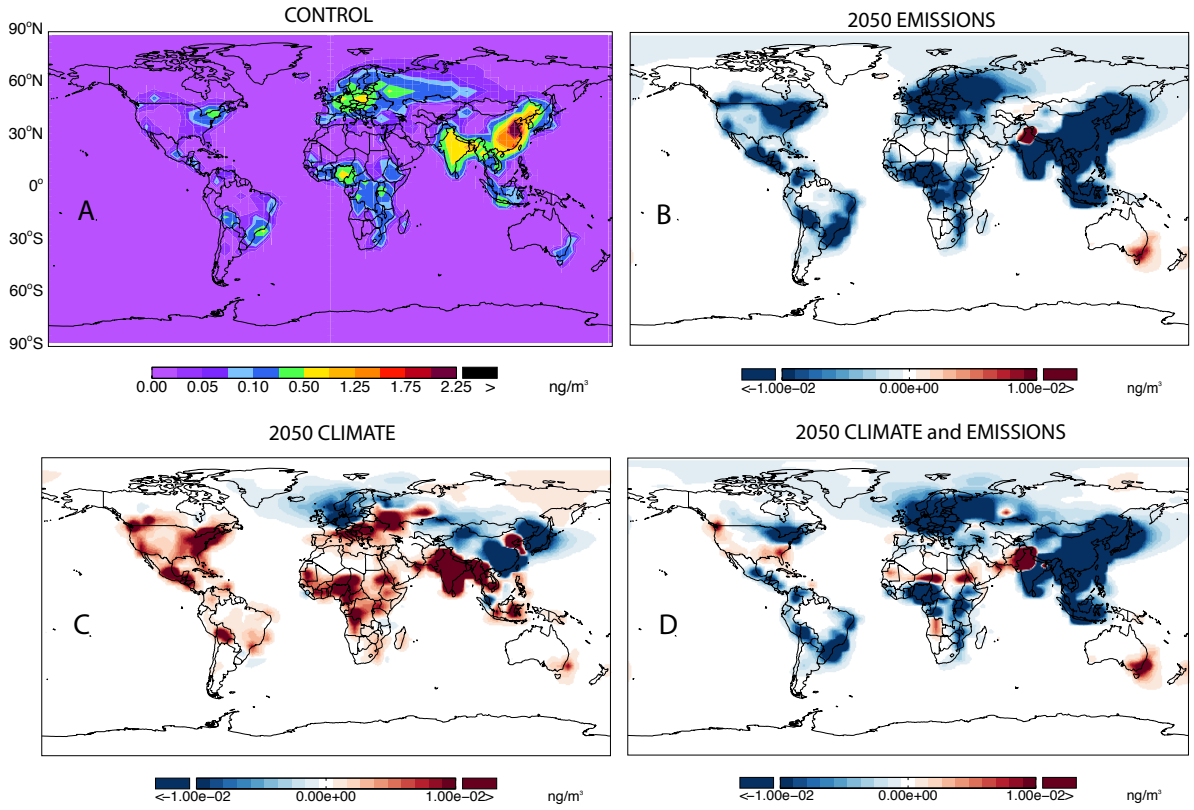

Figure S10. PYR concentrations under (A) the control; concentration differences between the control and simulations under (B) future emissions; (C) future climate; (D) future climate, future emissions. Red marks increases, blue marks decreases.

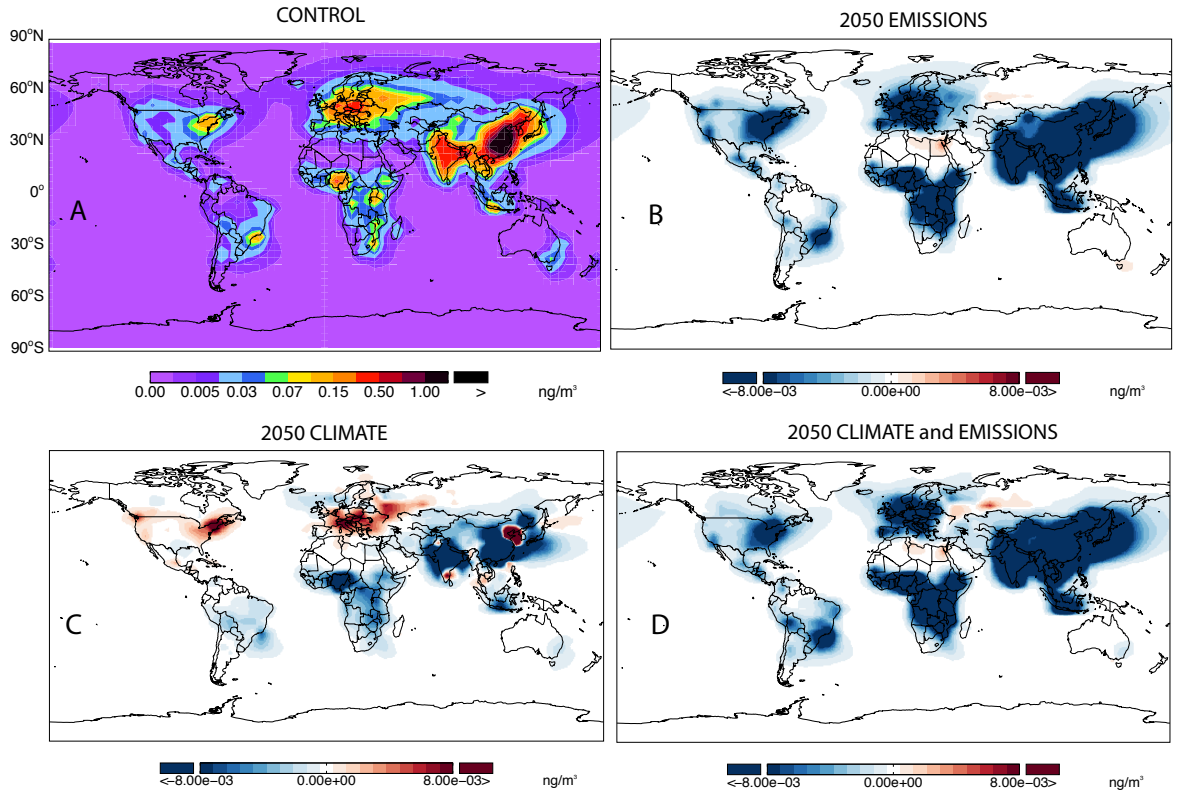

Figure S11. BaP concentrations under (A) the control; concentrations differences between the control and simulations under (B) future emissions; (C) future climate; (D) future climate, future emissions. Red marks increases, blue marks decreases.

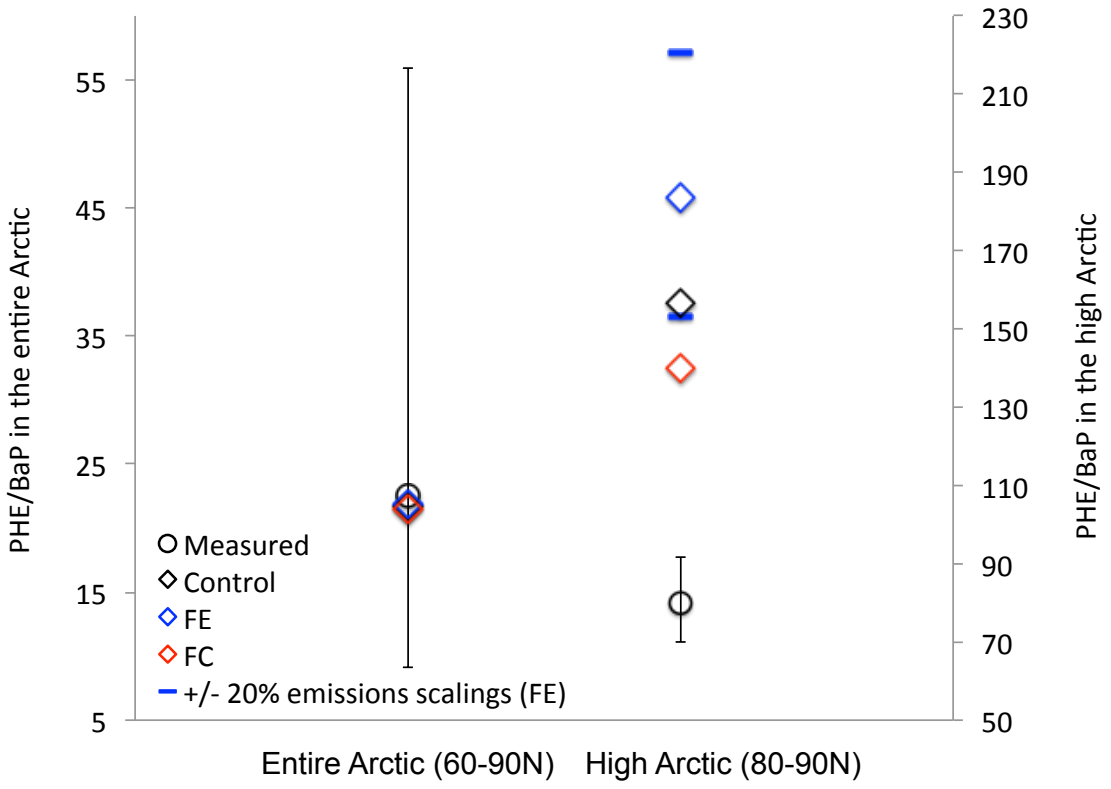

Figure S12. Comparison of simulated mean annual PHE/BaP (control, FE, and FC) to observed in both the entire and high Arctic. Geometric means and standard errors of observed concentrations are from Arctic sites listed in Table 1 of Friedman and Selin[33]. Also shown for the high Arctic is the range of PHE/BaP under FE when anthropogenic emissions are scaled +/-20% of the default projections (blue bars). The relatively large standard error from observations in the entire Arctic forces the symbols representing the means to overlap; the symbol representing the ratio in the control simulation (black diamond) is obscured by the symbols from the FE and FC simulations.

Literature Cited

1. Mackay, D.; Paterson, S. Evaluating the multimedia fate of organic chemics: A level III fugacity model. *Environ. Sci. Technol.* **1991,** *25*, 427-436.

2. Howsam, M.; Jones, K. C.; Ineson, P. Dynamics of PAH deposition, cycling and storage in a mixed- deciduous (Quercus-Fraxinus) woodland ecosystem. *Environ. Poll.* **2001,** *113*, 163-176.

3. Smith-Downey, N.; Sunderland, E.; Jacob, D. Anthropogenic impacts on global storage and emissions of mercury from terrestrial soils: insights from a new global model. *J. Geophys. Res.* **2010,** *115*, G03008.

4. Wang, W.; Simonich, S.; Giri, B.; Chang, Y.; Zhang, Y.; Jia, Y.; Tao, S.; Wang, R.; Wang, B.; Li, W.; Cao, J.; Lu, X. Atmospheric concentrations and air-soil exchange of polycyclic aromatic hydrocarbons (PAHs) in remote, rural village and urban areas of Beijing-Tianjin region, North China. *Sci. Total Environ.* **2011,** *409*, 2942-2950.

5. Cabrerizo, A.; Dachs, J.; Moeckel, C.; Ojeda, M.-J.; Caballero, G.; Barceló, D.; Jones, K. C. Ubiquitous net volatilization of polycyclic aromatic hydrocarbons from soils and parameters influencing their soil-air partition. *Environ. Sci. Technol.* **2011,** *45*, 4740-4747.

6. Liu, G.; Yu, L.; Li, J.; Liu, X.; Zhang, G. PAHs in soils and estimated air-soil exchange in the Pearl River Delta, South China. *Environ. Monit. Assess.* **2011,** *173*, 861-870.

7. Harner, T.; Bidleman, T. F. Octanol-air partition coefficient for describing particle/gas partitioning of aromatic compounds in urban air. *Environ. Sci. Technol.* **1998,** *32*, 1494-1502.

8. Harner, T.; Bidleman, T. F.; Jantunen, L. M. M.; Mackay, D. Soil-air exchange model of persistent pesticides in the United States cotton belt. *Environ. Toxicol. Chem.* **2001,** *20*, 1612-1621.

9. Ribes, S.; Van Drooge, B.; Dachs, J.; Gustafsson, O.; Grimalt, J. O. Influence of soot carbon on the soil-air partitioning of polycyclic aromatic hydrocarbons. *Environ. Sci. Technol.* **2003,** *37*, 2675-2680.

10. Potter, C. S.; Randerson, J. T.; Field, C. B.; Matson, P. A.; Vitousek, P. M.; Mooney, H. A.; Klooster, S. A. Terrestrial ecosystem production: A process model based on global satellite and surface data. *Global Biogeochem. Cycles* **1993,** *7*, 811-841.

11. McLachlan, M. S.; Czub, G.; Wania, F. The influence of vertical sorbed phase transport on the fate of organic chemicals in surface soils. *Environ. Sci. Technol.* **2002,** *36*, 4860-4867.

12. Cousins, I. T.; Mackay, D. Strategies for including vegetation compartments in multimedia models. *Chemosphere* **2001,** *44*, 643-654.

13. Cousins, I. T.; Mackay, D. Transport parameters and mass balance equations for vegetation in Level III fugacity models. Internal report published on the website of the Canadian Environmental Modelling Centre (http://www.trent.ca/envmodel/). **2000**.

14. Simonich, S. L.; Hites, R. A. Vegetation-atmosphere partitioning of polycyclic aromatic hydrocarbons. *Environ. Sci. Technol.* **1994,** *28*, 939-943.

15. Tremolada, P.; Burnett, V.; Calamari, D.; Jones, K. C. Spatial distribution of PAHs in the UK atmosphere using pine needles. *Environ. Sci. Technol.* **1996,** *30*, 3570-3577.

16. Ma, Y.-G.; Lei, Y.; Xiao, H.; Wania, F.; Wang, W.-H. Critical review and recommended values for the physical-chemical property data of 15 polycyclic aromatic hydrocarbons at 25 °C. *J. Chem. Eng. Data* **2010,** *55*, 819-825.

17. Lohmann, R.; Lammel, G. Adsorptive and absorptive contributions to the gas-particle partitioning of polycyclic aromatic hydrocarbons: State of knowledge and recommended parametrization for modeling. *Environ. Sci. Technol.* **2004,** *38*, 3793-3803.

18. Schwarzenbach, R. P.; Gschwend, P. M.; Imboden, D. M., *Environmental Organic Chemistry*. 2nd ed.; 2003.

19. Brubaker, W. W.; Hites, R. A. OH reaction kinetics of polycyclic aromatic hydrocarbons and polychlorinated dibenzo-p-dioxins and dibenzofurans. *J. Phys. Chem. A* **1998,** *102*, 915-921.

20. EPA, U. S. Estimation Programs Interface Suite for Microsoft Windows, v 4.10. United States Environmental Protection Agency, Washington DC, USA. **2011**.

21. Kahan, T. F.; Kwamena, N.-O. A.; Donaldson, D. J. Heterogeneous ozonation kinetics of polycyclic aromatic hydrocarbons on organic films. *Atmos. Environ.* **2006,** *40*, 3448-3459.

22. Park, R. J.; Jacob, D. J.; Chin, M.; Martin, R. V. Sources of carbonaceous aerosols over the United States and implications for natural visibility. *J. Geophys. Res.* **2003,** *108(D12)*, 4355.

23. IMAGE. The Image 2.2 implementatino of the SRES scenarios, *Publ. 481508018*, [CD-ROM], Natl. Inst. for Public Health and the Environ., Bilthoven, Netherlands, July. **2001**.

24. Wu, S.; Mickley, L. J.; Jacob, D. J.; Rind, D.; Streets, D. G. Effects of 2000-2050 changes in climate and emissions on global tropospheric ozone and the policy-relevant background surface ozone in the United States. *J. Geophys. Res.* **2008,** *113*, D18312.

25. Streets, D. G.; Bond, T. C.; Lee, T.; Jang, C. On the future of carbonaceous aerosol emissions. *J. Geophys. Res.* **2004,** *109*, D24212.

26. Pye, H. O. T.; Liao, H.; Wu, S.; Mickley, L. J.; Jacob, D. J.; Henze, D. K.; Seinfeld, J. H. Effect of changes in climate and emissions on future sulfate-nitrate-ammonium aerosol levels in the United States. *J. Geophys. Res.* **2009,** *114*, D01205.

27. Wu, S.; Mickley, L. J.; Leibensperger, E. M.; Jacob, D. J.; Rind, D.; Streets, D. G. Effects of 2000-2050 global change on ozone air quality in the United States. *J. Geophys. Res.* **2008,** *113*, D06302.

28. Knorr, W.; Lehsten, V.; Arneth, A. Determinants and predictability of global wildfire emissions. *Atmos. Chem. Phys.* **2012,** *12*, 6845-6861.

29. Beyer, A.; Wania, F.; Gouin, T.; Mackay, D.; Matthies, M. Selecting internally consistent physicochemical properties of organic compounds. *Environ. Toxicol. Chem.* **2002,** *21*, 941-953.

30. Odabasi, M.; Cetin, E.; Sofuoglu, A. Determination of octanol-air partition coefficients and supercooled liquid vapor pressures of PAHs as a function of temperature: Application to gas-particle partitioning in an urban atmosphere. *Atmos. Environ.* **2006,** *40*, 6615-6625.

31. Shiu, W.-Y.; Ma, K.-C. Temperature dependence of physical-chemical properties of selected chemicals of environmental interest. I. Mononuclear and polynuclear aromatic hydrocarbons. *J. Phys. Chem. Ref. Data* **2000,** *29*, 41-130.

32. Biermann, H. W.; Mac Leod, H.; Atkinson, R.; Winer, A. M.; Pitts, J. N. Kinetics of the gas-phase reactions of the hydroxyl radical with naphthalene, phenanthrene, and anthracene. *Environ. Sci. Technol.* **1985,** *19*, 244-248.

33. Friedman, C. L.; Selin, N. E. Long-range atmospheric transport of polycyclic aromatic hydrocarbons: A global 3-D model analysis including evaluation of Arctic sources. *Environ. Sci. Technol.* **2012,** *46*, 9501-9510.

34. Peters, G. P.; Nilssen, T. B.; Lindholt, L.; Eide, M. S.; Glomsrød, S.; Eide, L. I.; Fuglestvedt, J. S. Future emissions from shipping and petroleum activities in the Arctic. *Atmos. Chem. Phys.* **2011,** *11*, 5305-5320.